CGER-I016-'94

CGER'S SUPERCOMPUTER ACTIVITY REPORT

Vol.2-1993

Center for Global Environmental Research

National Institute for Environmental Studies
Environment Agency of Japan

Supercomputer Steering Committee (FY1993)

Prof. Haruhisa Ishida (University of Tokyo)
Prof. Taroh Matsuno (University of Tokyo*1)
Prof. Hisayoshi Morisugi (Gifu University)
Dr. Shuzo Nishioka (CGER/NIES: Chairman)
Dr. Kenzo Takano (Ex-Professor of University of Tsukuba)
Dr. Tatsushi Tokioka (Meteorological Research Institute*2)
Prof. Takeo Yamamoto (University of Library and Information Science)
Mr. Yoshio Yamanaka (EIC/NIES*3)
Dr. Masayuki Yasuno (NIES)
[*1 present affiliation: Hokkaido University; *2 present affiliation: Japan Meteorology Agency; *3 present affiliation: Osaka Gakuin University]

Coordination for Resource Allocation of the Supercomputer (CGER/NIES) (FY1993)

Dr. Shuzo Nishioka (Director)
Dr. Kuninori Otsubo
Dr. Hideo Harasawa
Mr. Tokuya Wada*4
[*4 present affiliation: Agency of Industrial Science and Techonology/MITI]

Maintenance of the Supercomputer System (EIC/NIES) (FY1993)

Mr. Yoshio Yamanaka (Director)
Dr. Shigenobu Abe (Head)
Mr. Kunihiko Shirai*5
Mr. Hideaki Abe
Mr. Koji Oishi
[*5 present affiliation: Management and Coordination Agency]

Operation of the Supercomputer System

System Engineers of NEC

Editors

Dr. Kuninori Otsubo (Chief)
Dr. Hideo Harasawa
Mr. Kunihiko Yamazaki

Center for Global Environmental Research
National Institute for Environmental Studies
16-2, Onogawa, Tsukuba, Ibaraki 305, Japan
Telephone: +81-298-51-6111
Facsimile: +81-298-58-2645

Copyright 1994

NIES: National Institute for Environmental Studies
CGER: Center for Global Environmental Research
EIC: Environmental Information Center

Foreword

The Center for Global Environmental Research (CGER) was established in October 1990 in the Environment Agency of Japan's National Institute for Environmental Studies (NIES), to contribute broadly to the elucidation and solution of pressing environmental problems.

CGER provides research-support facilities such as databases and a supercomputer for researchers in various fields. CGER's supercomputer system is operated primarily for research concerning global environmental issues. The system is open generally to environmental researchers worldwide.

Proposed research programs are evaluated by the Supercomputer Steering Committee which consists of leading scientists in climate modeling, atmospheric chemistry, oceanic circulation and computer science. After project approval, certification for system usage is provided.

Volume 2 of this annual report compiles the selected research activities of the users of CGER's supercomputer during fiscal 1993. The respective research papers published here are interim progress reports, not necessarily finished products suitable for publication as full papers after program completion. The papers are classified into four categories; Climate Modeling, Atmospheric and Oceanic Environment Modeling, Geophysical Fluid Dynamics and Others. The report also includes an overview of the supercomputer.

We hope this report provides you with useful information on the global environmental research being conducted on our supercomputer. Please do not hesitate to comment freely, directly to the Research Integration Section of CGER, so that subsequent reports both truly reflect and effectively foster cooperation throughout the community of scientists using this supercomputer.

December 1994

Yoshinori Ishii
Executive Director
Center for Global Environmental Research
National Institute for Environmental Studies

Preface

The Center for Global Environmental Research (CGER) of the Environment Agency of Japan's National Institute for Environmental Studies (NIES) provides research-support facilities such as a supercomputer and databases for global environmental research activities. CGER's supercomputer is open to researchers internationally for any global environmental research applications. Users need to be certified for such usage every fiscal year. CGER is responsible for efficient and adequate allocation of supercomputer resources, such as CPU time and memory, to each research subject, in accordance with the research plan recommended by the Supercomputer Steering Committee consisting of nine scientists.

NIES's Environmental Information Center (EIC) manages routine operation of the supercomputer system. This system is operated with close and cordial communication between users and the managing staff. Daily consultation by the system engineers also improves communication.

Progress in selected research projects is presented at an annual workshop. These workshops also offer opportunities for communication among users and discussion of the results obtained with scientists of the global environmental area.

The system's CPU time and memory have been completely occupied in fiscal year 1993 (from April 1993 to March 1994), demonstrating that the needs of researchers to use the facility have been very high and that users from national research institutes and universities have fully utilized the system. We provided high-priority resource allocation to a group at the Meteorological Research Institute, in consideration of their prospective contribution to international frontier research activities on climate change modeling after assessing their research plan.

This report is the second publication of activities by the supercomputer facility, which aims at disseminating selected research progress from FY 1993. We hope it contributes to further progress in global change research and efforts for global environmental conservation.

December 1994

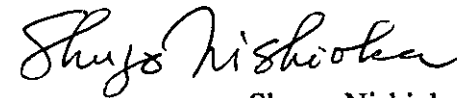

Shuzo Nishioka
Director
Center for Global Environmental Research
National Institute for Environmental Studies

Contents

1. Climate Modeling

(GCM: General Circulation Model)

Transient Response Study to the Gradual Increase of Atmospheric CO_2 Concentration with a Coupled Atmosphere-Ocean Model Developed at the Meteorological Research Institute

Contact Person	Tatsushi Tokioka Climate Research Department, Meteorological Research Institute Present affiliation: Japan Meteorological Agency
Research Organization	Akira Noda, Shinji Nakagawa, Tatsuo Motoi, Seiji Yukimoto, Akio Kitoh, Yoshinobu Nikaidou Climate Research Department, Meteorological Research Institute

Keywords climate model, climate change, global warming

1. Introduction

Transient response studies to a gradual increase of atmospheric CO_2 have been reported by four groups so far (IPCC, 1992). They are by GFDL (Stouffer *et al.*, 1989; Manabe *et al.*, 1991; Manabe *et al.*, 1992; Delworth *et al.*, 1993), NCAR (Meehl *et al.*, 1993), UKMO (Murphy, 1992) and MPI (Cubasch *et al.*, 1992). All these models do not have fine horizontal resolutions of ocean enough to simulate El Niño phenomena. There are debates on how El Niño phenomena change under the global warming. GFDL's group shows that the amplitude of sea surface temperature (SST) anomalies during ENSO-like events in the CO_2-warmed climate is slightly reduced compared to that in a control run (Knutson and Manabe, 1994). MPI's group also speculates less active El Niño under the warming process (Lunkeit *et al.*, 1993), while NCAR's group speculates opposite (Meehl *et al.*, 1993). On the other hand, UKMO's group shows no significant changes in the equatorial SST variability between the transient and control simulations (Tett, 1994). However, these models have not necessarily simulated whole cycle of El Niño phenomena well in their simulations. Unless we perform simulations of transient response to the gradual increase of CO_2 with a model which does simulate El Niño phenomena, no persuasive conclusion can be reached.

Some models used for transient response studies do not simulate either sea ice thickness or distribution, or both of them well. In one model, sea ice thickness in the Antarctic ocean in September is more than 3 m in some area (Manabe *et al.*, 1992). However, observation shows that preferred thickness of the sea ice in the Antarctic ocean are 40-60 cm in austral midwinter (Wadhams *et al.*, 1987). In another model, sea ice in the Antarctic ocean has almost disappeared even in September (Murphy, 1992). If a model does not simulate either thickness or distribution of sea ice or both of them, it is quite likely that the model fails to evaluate feedback processes related to sea ice quantitatively, and produces some errors in predicting possible future climate changes due to the increase of CO_2.

In this report, we describe results of a simulation of transient response to the gradual increase of CO_2 with a climate model which has been improved in the aspects mentioned above. Full description of the present results will be presented later in separate reports.

2. Model

Atmospheric part of the model (AGCM) is basically identical to the MRI-GCM-I (Tokioka *et al.*, 1984) except for radiation part. Horizontal resolution of the AGCM is 5° by 4° in longitudinal and latitudinal directions, respectively. There are 15 vertical layers with the top at 1hPa. Shortwave radiation calculation is based on Lacis and Hansen (1974) and longwave radiation calculation on Shibata and Aoki (1989). Five types of clouds are diagnostically determined: *i.e.*, penetrative cumulus cloud, middle level convective cloud, planetary boundary layer stratus cloud, large-scale condensation cloud and cirrus anvil cloud. Partial cloudiness is allowed for the convective clouds. Effect of sub-grid-scale topography on the grid scale flow is included as gravity-wave drag following Palmer *et al.* (1986) with quantitative adjustment described by Yagai and Yamazaki (1988). Thermodynamic and hydrological processes of land surface are based on multi-layer soil model. There are four layers with the bottom at 10 m depth. Ground temperature, soil moisture and frozen soil moisture are predicted at each level.

Oceanic part of the model (OGCM) is a global ocean general circulation model developed at the Meteorological Research Institute (MRI). The model is now extended to include realistic ocean bottom topography and variable resolution in the meridional direction, ranging from 0.5° at the equator to 2.0° at 12° latitude and further poleward (see Fig.1). The resolution in the longitudinal direction is 2.5° and there are 21 vertical layers, 6 of which are located in the first 300 m. The Mellor-Yamada level 2 turbulence closure scheme is included to simulate oceanic mixed layer. The lateral eddy viscosity and diffusivity are set to 2.0×10^9 cm^2/s and 5.0×10^7 cm^2/s, respectively, between 78°N and 78°S. The vertical eddy viscosity and diffusivity are calculated following Mellor and Yamada (1974, 1982) and Mellor and Durbin (1975).

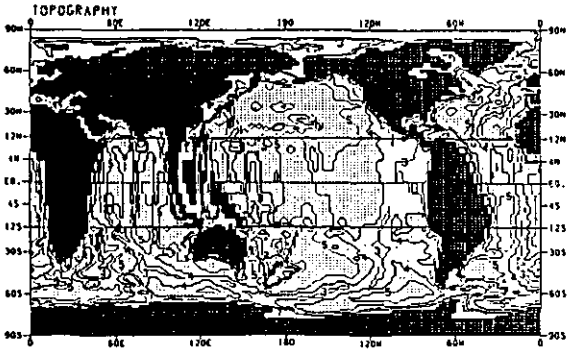

Fig. 1 The horizontal resolution and topography of the OGCM. Variable resolution is used in the meridional direction, ranging from 0.5° at the equator to 2.0° at 12° latitude and further poleward. Contour interval is 1000 m.

Sea ice model is included. The model predicts compactness (areal coverage ratio of sea ice) as well as thickness and surface temperature of sea ice. The movement of sea ice is predicted by considering stress from oceanic current at the first level of the ocean. Energy exchanges through the surface are calculated both in the sea ice area and "leads" separately and are weighted with the respective coverage ratio. The model can simulate seasonal variation of sea ice compactness and thickness realistically not only in the Arctic but also in the circum-Antarctic area. The performances of the sea ice model will be described fully in a separate paper.

The current climate model has different horizontal resolution between the AGCM and the OGCM. Furthermore, we predict areal coverage ratio of sea ice in each ocean grid, as explained above. In calculating surface energy fluxes, we linearly add energy fluxes calculated between atmosphere and a part of surface area (which is either land , open ocean or sea ice) of one atmospheric grid with the areal ratio of the part to the atmospheric grid. We allow partial coverage of land at both coastal and island grids.

3. Experiment

Two runs were performed, *i.e.*, a run with a fixed atmospheric CO_2 concentration (C run) at 345 ppmv and a run with a gradual increase of CO_2 at a compound rate of 1%/yr (G run). This increasing rate of CO_2 roughly corresponds to the actual increase of radiative forcing due to the increase of several greenhouse gases and has been used in other studies (Stouffer *et al.*, 1989; Manabe et al, 1991; Murphy, 1992). In both C and G runs flux corrections in the surface energy and water fluxes were included to predict realistic SST and surface salinity. Runs were continued up to the year 70 in both C and G runs.

4. Results and Remarks

In this paper, most analyses will be based on the difference between G run and C run (G-C). C run has succeeded in reproducing not only basic climatological characteristics of time mean fields including SST but also variability from interannual to interdecadal time scales.

Figure 2 shows the time evolution of area-averaged, annual-mean surface air temperature for the C run and the G run. There remains a weak secular trend in the Southern Hemisphere, which is, however, small enough to detect the CO_2 warming signal. The globally averaged surface air temperature increases 1.6 °C during the seventy-year period.

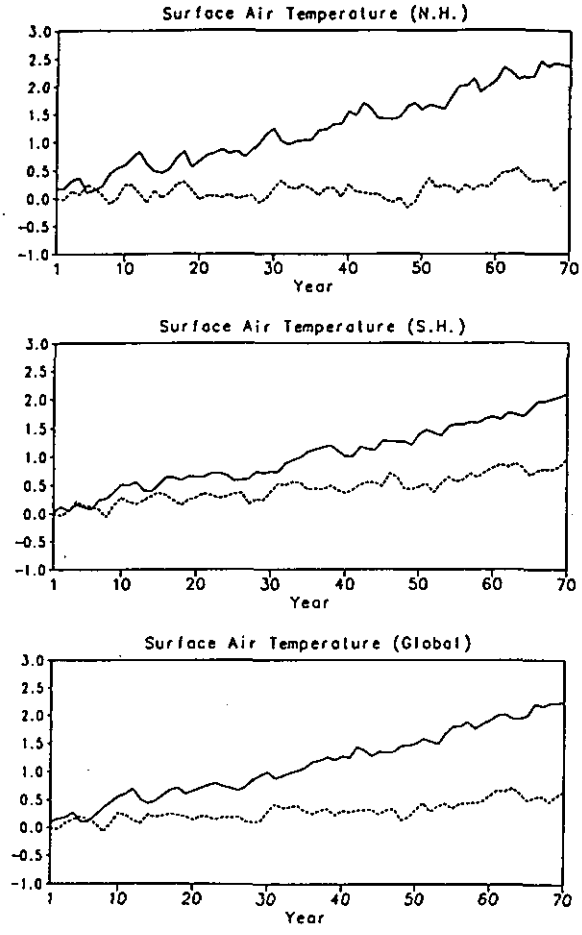

Fig. 2 Time evolution of annual-mean surface air temperature averaged over the Northern Hemisphere (top), the Southern Hemisphere (middle) and the globe (bottom). Solid and dashed lines indicate the G run and the C run, respectively. The zero point is the annual mean for the first year of the C run. In the G run, CO_2 concentration is increased at a compound rate of 1%/yr, while it is fixed in the C run.

Figure 3 shows the latitude-time section of zonally averaged surface air temperature change. The

delay of temperature rise in the Southern Hemisphere especially around 50°S is dominant, as already pointed out by Stouffer *et al.* (1989). It is also worthy to point out that the rise of surface air temperature in the Arctic region is rather small up to the year 50. However, it starts to increase at a larger rate than before after the year 50. This has not been stressed before although similar tendency is seen in Fig.1 of Stouffer *et al.* (1989). Murphy (1992) and Cubasch *et al.* (1992) have mentioned initial slow rise in the globally averaged surface air temperature in relation to the initial spin up problem or the cold start problem (Hasselmann *et al.*, 1992). However, the globally averaged surface air temperature increase almost linearly in Fig.2 so that the cold start problem is irrelevant to the present experiment.

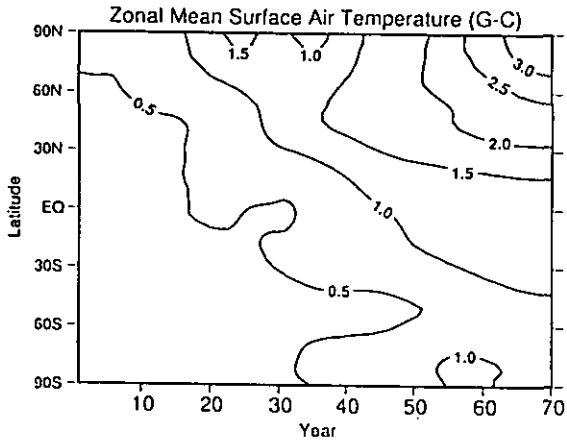

Fig. 3 Latitude-time section of zonally averaged surface air temperature difference, which is taken between the G run and the C run at the same time instance. Periods shorter than 12 years have been filtered out.

Figure 4 shows the temporal variation of sea ice volume averaged over the polar region between 75°N and 90°N for the C and G runs. It can be seen that there is interdecadal variation as well as interannual variation in the simulated Arctic sea ice, and that the interdecadal variation has an amplitude comparable with that due to the doubled CO_2 radiative forcing around the year 70. This indicates that the temporal evolution of CO_2 warming is much affected by not only amplitude but also phase of the natural variability in sea ice. In the present experiment, a transition from the positive to the negative anomaly phase in sea ice volume happens to be around the year 50, so that a delay (acceleration) of the warming is found before (after) that time.

The clear difference in the meridional structure of temperature change before and after around the year 50 shows that atmospheric response pattern to the gradual increase of CO_2 is not constant in time but is a function of time.

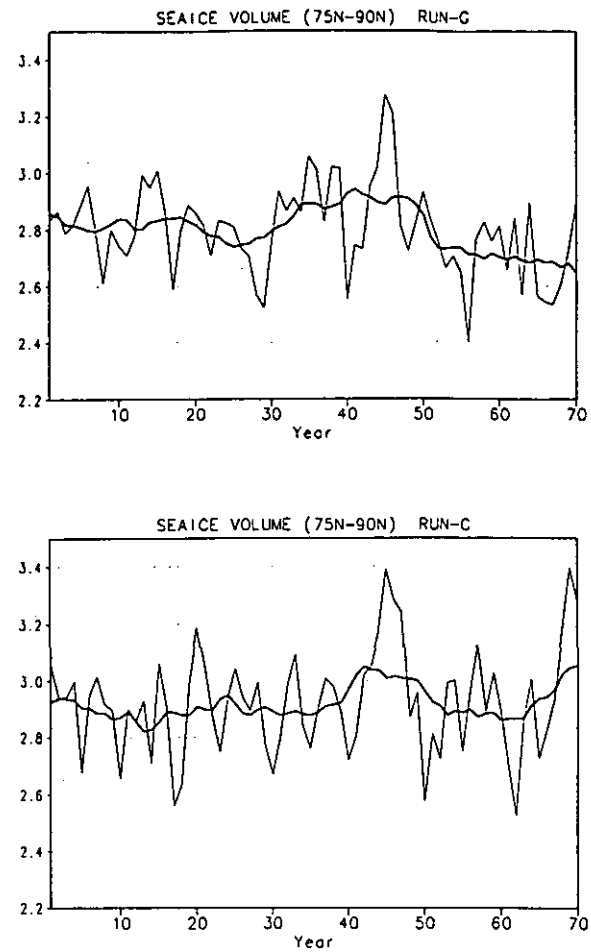

Fig. 4 Temporal variation of sea ice volume averaged over the area between 75°N and 90°N for the G run (top) and the C run (bottom). Thin and thick lines indicate annual mean and 11-year running mean, respectively.

Figure 5 shows the spatial pattern of the first mode of empirical orthogonal function (EOF) analysis for annual mean SST difference (G-C) and the time variation of the coefficient. Periods shorter than 12 years have been filtered out for the SST difference. The first EOF of SST of the G run is almost identical to that shown in Fig.5. The coefficient shows an overall linear increasing trend over 70 years, indicating that this is a response mode to the gradual increase of CO_2. The SST rise is large in the sea of Okhotsk as the sea ice has partially disappeared. This is expected from the fact that the area is located near the southernmost boundary of sea ice formation in the Northern Hemisphere, so that the sea ice-albedo feedback may work early and effectively. Between 40°S and 60°S where most area is covered by ocean, SST rise is generally delayed as in other studies (Stouffer *et al.*, 1989; Murphy, 1992; Cubasch *et al.*, 1992). There is dominant warming in the North Pacific, the North Atlantic and the subtropical latitudes of the Southern Hemisphere.

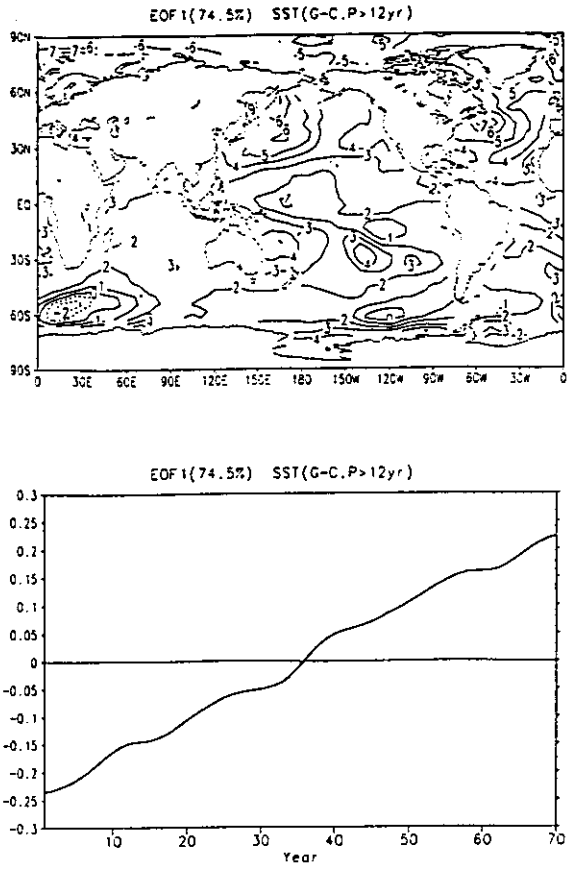

Fig. 5 The first mode of empirical orthogonal function (EOF) analysis of the annually averaged sea surface temperature (SST) difference between the G run and the C run. (top) Spatial pattern, (bottom) time evolution of the amplitude of the mode. Periods shorter than 12 years have been filtered out. Contribution of this mode is shown in the parentheses at the top of the figure.

Figure 6 is the same as Fig.5 but for surface air temperature. Spatial variation over the ocean is almost identical to that in Fig.5. There are pronounced increase of temperature over the continent in mid-latitudes in both hemispheres, especially in the sub-tropics. This land-sea contrast of the warming is explained by Saito and Tokioka (1994). The most dominant increase is found over the sea of Okhotsk due to the disappearance of sea ice as mentioned above. Although the temperature increase in high latitudes of the Northern Hemisphere is dominant, it is not so large as in Stouffer *et al.* (1989). The increase occurs mostly in the last 20 years as shown in Fig.3. In the present model, sensible and latent fluxes from leads increase in proportion to the increase of area of leads when SST increases. This works as a negative feedback to SST rise. Another negative feedback works in sea ice because heat conduction increases as ice thickness decrease. However, the feedback in the lead region is much stronger than that in the sea ice region. The difference in the magnitude of the negative feedback may be responsible for the less temperature rise in the Arctic in the present simulation than in the GFDL's where no lead is considered in the sea ice model.

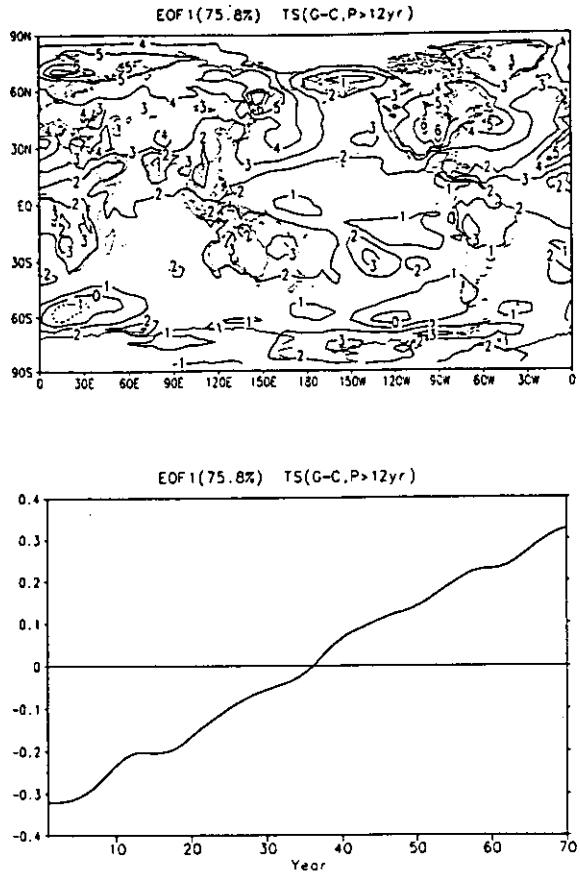

Fig. 6 The same as in Fig.5 but for surface air temperature.

Figure 7 is the second EOF of SST of the G run. This mode has large amplitudes in the Pacific. The most notable feature is a wedge like pattern in the central Pacific, with opposite polarity in the north-western and the south-western mid Pacific. We observe almost identical spatial pattern in the first (not shown) and the second EOF modes of SST in C and G runs, respectively, indicating that this is an internal mode of the climate system.

Figure 8 shows time evolution of the amplitude of the first EOF of SST of the C run. Both of the first and the second SST modes in C and G runs, respectively, show dominant 6 year cycles, which is close to the typical time scale of El Niño, and interdecadal modulations of them with about 30 years. Another important point to be noted is that the interdecadal time evolutions of both modes are almost identical to each other up to the year 30 or so. In another words, this type of variation could be affected little by the increase of CO_2 concentration, and thus could be predicted about 30 years ahead.

The mechanisms of the variability of this mode is being studied and will be reported separately from this study. This mode has a characteristic structure in the Pacific sub-tropical gyre down to about 500 m deep, which will be the main reason to allow such a long time predictability over 30 years.

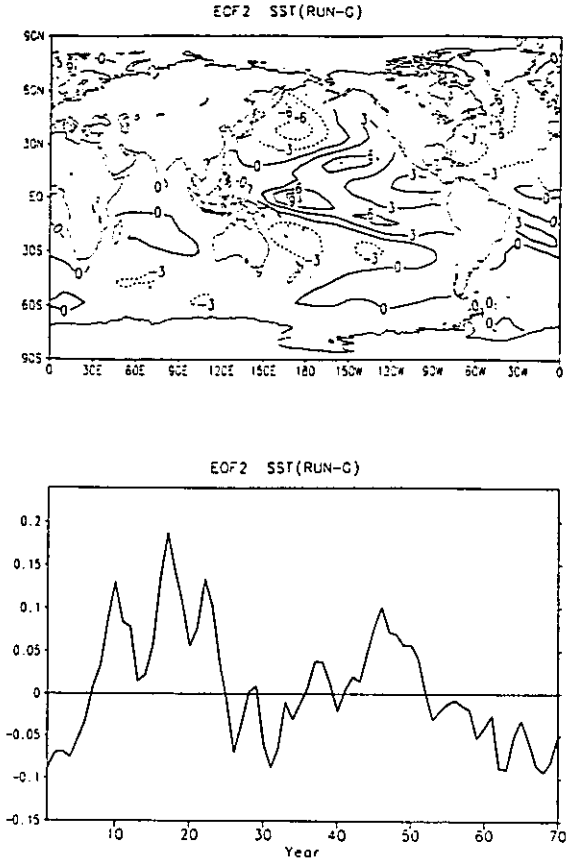

Fig. 7 The second mode of EOF analysis of the annually averaged SST for the G run. No low-pass filter has been applied.

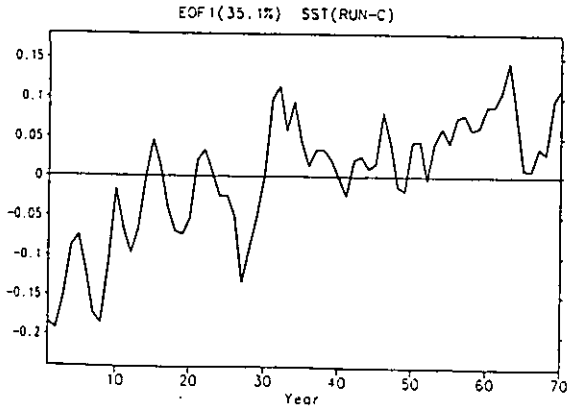

Fig. 8 Time evolution of the amplitude of the first EOF of SST of the C run. The spatial pattern of this mode is almost identical to that in Fig.7.

Figures 9 and 10 show the first and the second EOF, respectively, of the observed annually averaged SST data, which are combinations of the COADS data (before 1985) and the JMA analyses (after 1986). The first mode (Fig.9) has several common characteristic features to those of Fig.7. As its time evolution shows, there is a kind of jump in the latter half of 1970s. Before this, it remains negative. However, it remains positive after that. Above normal SST in the eastern equatorial Pacific, and below normal SST in the Northern mid Pacific observed in recent years are captured by this mode.

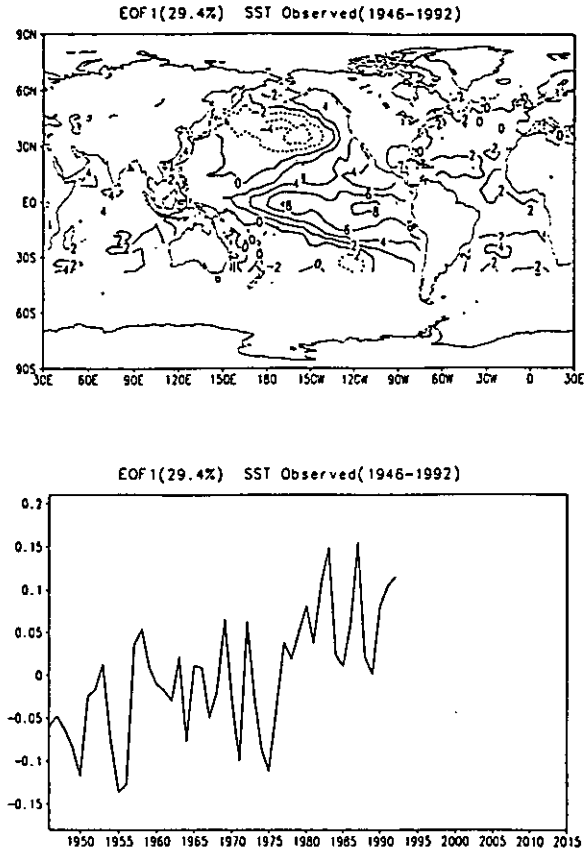

Fig. 9 The same as in Fig.7 but for the first EOF for the observed SST, which is a combination of COADS data from 1946 to 1985 and the JMA analysis from 1986 to 1992.

The second mode (Fig.10) has a large amplitude in the equatorial eastern Pacific area similar to that of the mature stage El Niño. El Niño seems to be splitted into the first and the second modes. Although a similar coupled model to the present one has succeeded in simulating El Niño phenomenon (Nagai *et al.*, 1992), enhanced warming in the eastern equatorial Pacific has not been captured well in the model. This might explain the reason why the present model does not have a mode corresponding to the one shown in Fig.10.

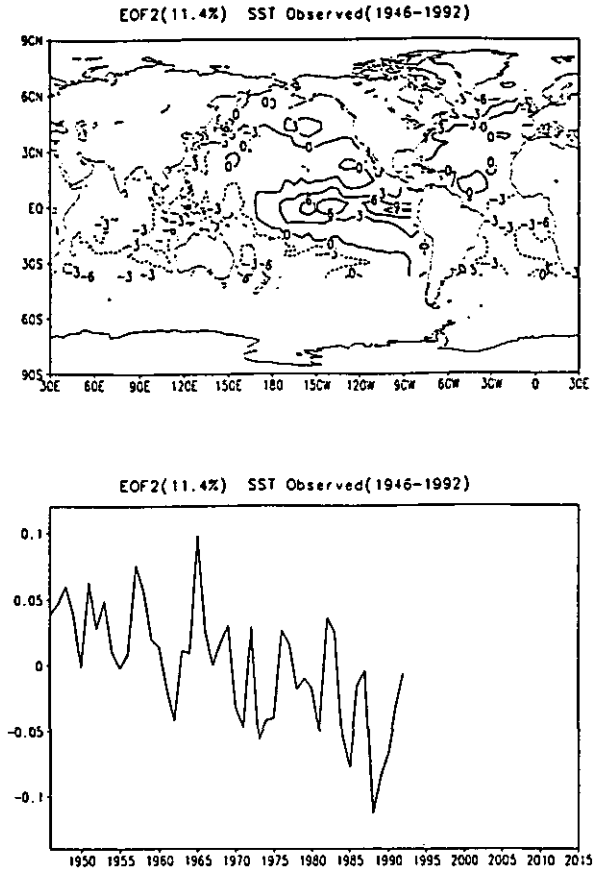

Fig. 10 The same as in Fig.9 but for the second EOF.

Quick comparison of variability in El Niño time scale between time evolutions of Figs.7 and 8 does not show clear differences. Here we do not say any conclusive statements on the change of El Niño phenomena due to the increase of CO_2. This point will be studied further separately.

5. Summary

A transient response experiment to the gradual increase of atmospheric CO_2 concentration at a compound rate of 1 %/yr has been performed with a coupled atmosphere-ocean general circulation model developed at the Meteorological Research Institute. The model is characterized with two aspects; one is relatively high resolution of the oceanic part in low latitudes to simulate El Niño phenomena, and the other is an elaborate sea ice model to simulate seasonal variation of sea ice coverage and thickness reasonably.

Time integration has been performed up to 70 years when the CO_2 concentration doubles. The globally averaged surface air temperature increases 1.6 °C during this period. Atmospheric response to the CO_2 increase is slow in the Southern Hemisphere and over oceanic area, as were already pointed out. However, surface air temperature increase in the Arctic region and over the surrounding continent is not much dominant up to the year 50. From the year 50 to 70, surface air temperature in the Arctic area starts to increase rapidly. Variation in sea ice with interdecadal time scales is found both in the transient and in the control run. A transition phase from the positive to negative anomaly of the interdecadal variation has occurred around the year 50. The variation is coupled with the constantly increasing CO_2 radiative forcing to result in the rapid warming after the year 50. This clearly indicates that atmospheric response pattern to CO_2 increase is not only a function of space but also of time, and that it is largely affected by natural variability.

The most dominant air-sea coupled mode in the model is very close to what is observed through the analysis of sea surface temperature. This mode has interannual variations in the Pacific with a dominant period of about 6 years, which is close to the typical time scale of El Niño. It also shows variations of interdecadal time scales, with implication of predictability for a few decades.

Acknowledgments

The present study was performed as a part of the special study on the prediction of global warming sponsored by the Japan Meteorological Agency. A part of this study was supported also as "A Climate Sensitivity Study by Use of a Coupled Atmosphere-Ocean Model" by the Center for Global Environmental Research/ National Institute for Environmental Studies. Special thanks are extended to staff members of the CGER/NIES computer center for their assistance in running the coupled atmosphere-ocean model.

This report is submitted to Journal of the Meteorological Society of Japan.

References

Cubasch, U., K. Hasselmann, H. Höck, E. Maier-Reimer, U. Mikolajewicz, B.D. Santer and R. Sausen, 1992: Time-dependent greenhouse warming computations with a coupled ocean-atmosphere model. Clim. Dyn. 8, 55-69.

Delworth, T., S. Manabe and R.J. Stouffer, 1993: Interdecadal variations of the thermohaline circulation in a coupled ocean-atmosphere model. J.Climate, 6, 1993-2011.

Hasselmann, K., R. Sausen, E. Marier-Reimer and R. Voss, 1992: On the cold start problem of coupled atmosphere-ocean models. MPI Report No.83, MPI, Hamburg, 25pp.

IPCC, 1992: Climate Change 1992; The Supplementary Report to the IPCC Scientific Assessment. eds. J.T. Houghton, B.A. Callander and S.K. Varney, Cambridge Univ. Press, 200pp.

Knutson, T.R. and S. Manabe, 1994: Impact of increasing CO_2 on the Walker Circulation and ENSO-like phenomena in a coupled ocean-atmosphere model. Extended Abstracts of the Sixth Conference on Climate Variations, 23-28 January 1994, Nashville, 80-81.

Lacis, A.A. and J.E. Hansen, 1974: A parameterization for the absorption of solar radiation in the Earth's atmosphere. J. Atmos. Sci., 31, 118-133.

Lunkeit, F., R. Sausen and J.M. Oberhuber, 1993: Simulation of the transient greenhouse warming with the coupled atmosphere-ocean model ECHAM2/OPYC. Abstracts of IAMAP-IAHS '93, 11-23 July, 1993, Yokohama, M3-66.

Manabe, S., R.J. Stouffer, M.J. Spelman and K. Bryan, 1991: Transient responses of a coupled ocean-atmosphere model to gradual changes of atmospheric CO_2. Part I: Annual mean response. J. Climate, 4, 785-818.

Manabe, S., M.J. Spelman and R.J. Stouffer, 1992: Transient response of a coupled ocean- atmosphere model to gradual changes of atmospheric CO_2. Part II: Seasonal response. J. Climate, 5, 105-126.

Meehl, G.A., G.W. Branstator and W.M. Washington, 1993: Tropical Pacific interannual variability and CO_2 climate change, J. Clim., 6, 42-63.

Mellor, G.L. and T. Yamada, 1974: A hierarchy of turbulence closure models for planetary boundary layers. J. Atmos. Sci., 31, 1791-1806.

Mellor, G.L. and P.A. Durbin, 1975: The structure and dynamics of the ocean surface mixed layer. J. Phys. Oceanogr., 5, 718-728.

Mellor, G.L. and T. Yamada, 1982: Development of a turbulence closure model for geophysical fluid problems. Rev. Geophys. Space Phys., 20, 851-875.

Murphy, J.M., 1992: A prediction of the transient response of climate. Climate Res. Tech. Note, No.32, Hadley Centre.

Nagai, T., T. Tokioka, M. Endoh and Y. Kitamura, 1992: El Niño-Southern Oscillation simulated in an MRI atmosphere-ocean coupled general circulation model. J. Climate, 5, 1202-1233.

Palmer, T.N., G.J. Shutts, R. Swinbank, 1986: Alleviation of a systematic westerly bias in general circulation and numerical weather prediction models through an orographic gravity wave drag parameterization. Quart. J. Roy. Meteor. Soc., 112, 1001-1039.

Saito, M. and T. Tokioka, 1994: Some aspects of ocean/continental-scale climate changes under global warming produced by CO_2 increase. Extended Abstracts of the Sixth Conference on Climate Variations, 23-28 January 1994, Nashville, 82-86.

Shibata, K. and T. Aoki, 1989: An infrared radiative scheme for the numerical models of weather and climate. J. Geophys. Res., 94, 14923-14943.

Stouffer, R.J., S. Manabe and K. Bryan, 1989: Interhemispheric asymmetry in climate response to a gradual increase of atmospheric CO_2. Nature, 342, 660-662.

Tett, S.F.B., 1994: Simulation of El Niño/Southern Oscillation like variability in a global AOGCM and its response to CO_2 increase. Climate Research Technical Note, No. 45, Hadley Center.

Tokioka, T., K. Yamazaki, I. Yagai and A. Kitoh, 1984: A description of the Meteorological Research Institute atmospheric general circulation model (the MRI-GCM-I). Tech. Report No.13, Meteorol. Res. Inst., Japan, 249pp.

Wadhams, P., M.A. Lange and S.F. Ackley, 1987: The ice thickness distribution across the Atlantic Sector of the Antarctic Ocean in midwinter. J. Geophys. Res., 92C, 14,535-14,552.

Yagai, I. and K. Yamazaki, 1988: Effect of the internal gravity wave drag on the 12-layer MRI GCM January simulation. Report No. 12 of the Proceedings of the WGNE Workshop on Systematic Errors in Models of the Atmosphere, 19-23 September 1988, Working Group on Numerical Experimentation, Toronto, 8pp.

Ultra-high resolution modeling of the tropical atmosphere

Contact Person Kensuke Nakajima
Center for Climate System Research, University of Tokyo
Keywords cumulus convection, tropical atmosphere, numerical modeling, WISHE, CISK

1.Backgrounds

Importance of cumulus convection in the energy and hydrological cycle of the earth's atmosphere can never be over-emphasized. But its smallnesses in temporal and spatial scales compared to the scale of the global atmosphere as a whole prevent it from explicitly calculated in current generation of GCM's. Thus every GCM includes cumulus parameterization, which have many uncertainties that arise from our poor understandings on the interaction between large scale motions and the cumulus clouds.

To quantify the interaction between cumulus convection and large-scale(LS) motion, so called 'cumulus ensemble models'(CEM) had been used since early 1980's. It is a large domain (O(100km)) cloud convection model, where one imposes an 'observed' large-scale forcing and analyzes the results in a statistical manner. There remains, however, a critical defect in this CEM approach; in the real atmosphere the interaction between cumulus clouds and large-scale motion is two-way, whereas in CEM it is forced to be one-way (large-scale motion is cause and cumulus convection must be its result). This can be straightend by doing cumulus resolving GCM simulations, but computational resource requirement for such calculations is enormous (at least 1,000,000 times that is available today).

Although three-dimensional calculation covering whole glove is impossible, two-dimensional calculation is within the power of current generation vector supercomputer. In this paper I report a preliminary results of such attempt.

2. 2-D Direct simulation of Cumulus-Large Scale interaction

I constructed a two-dimensional cloud model that covers up to 16384km. Its high spatial resolution (2km) and incorporation of cloud microphysical processes allows cumulus convection to be represented explicitly. At the same time, the domain is as large as the longitudinal size of the pacific. Suface latent and sensible heat fluxes are supplied from the underlying fixed temperature ocean using bulk formulae. The troposphere of the model is cooled at a (basically) constant rate, crudely simulating the effect of radiation. The time marching can be continued 10days or longer with 24 hour CPU time using the SX-3 at CGER-NIES.

The construction of numerical model alone is not sufficient for examination of the cumulus-LS interaction; we must find a set-up where such interaction naturally occur. Wind induced surface heat exchange (WISHE) provides one of such mechanism, and Nakajima(1993) reported a simulation of WISHE disturbance. Here I mainly present results concerning wave-CISK, which is another example of cumulus-LS interaction. For complete decriptions of the results, see Nakajima(1994).

3.Wave-CISK experiment

Wave-CISK (Conditional Instability of Second Kind) is amplification of large scale internal waves through its interaction with cumulus convection. It has been studied in linear instability framework by many authors beginning from pioneering works by Yamasaki(1969), Y.Hayashi(1970) and Lindzen(1974). Many of them considered equatorial waves, but its essense is valid in 2-D framework which our numerical model can simulate.

The outcome of those linear theories contains two major difficulties. The first is that the growth rate is inversely proportional to wavelength of the disturbance, so that it explodes at zero wavelength and it does not predict 'preffered scale'. The second is that the results sensitively depends on the assumption on the relationship between cumulus activity and the LS motion which is not well-understood nor quantified, so that we cannot be very confident on the results of such theory. Therefore, in fact, whether 2-D direct calculation produce something that can be identified as wave-CISK or not is far from being obvious.

The success of WISHE experiment reported in Nakajima (1993) gives an important caution: one must carefully exclude WISHE if he or she wants to examine something other. So in this experiment, I hold the wind speed used in the surface flux calculation at a constant and homogeneous value in order to suppress the emergence of WISHE-related instabilities.

4.Results

a. Importance of vertical profile of body cooling in the troposphere

Linear theories in the past have been identified the vertical profile of heating by cumulus convection as an crutial factor. In this experiment, however, we can not specify the structure of cumulus heating a priori, because it is a part of the results of the experiments. Instead I change the vertical profile of the body cooling, expecting that the cumulus heating, balancing to the body cooling, will also change its vertical structure. I show here two cases, i.e., case HC where body cooling is enhanced in the upper levels, and case LC where it is enhanced in the lower levels. Based on the linear theories, wave-CISK is preffered in case HC. Both experiments are done using a model with 4,096 km horizontal domain size.

Fig.1 shows time-space distribution of rainfall in-

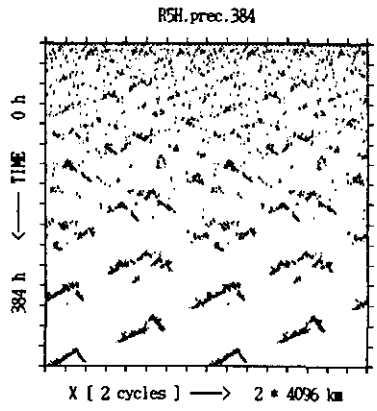

Figure 1: Time evolution of rainfall distribution in case HC. Two cycles of 4,096 km domain is shown from left to right. Time goes down from 0 h to 384 h.

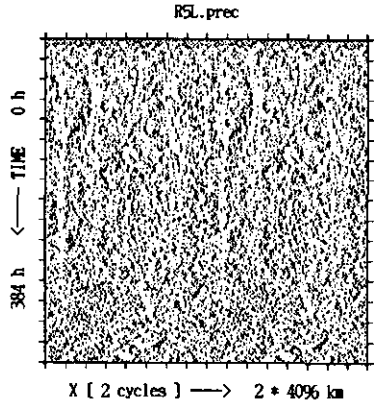

Figure 2: Same as Fig.1 but for case LC.

tensity for the case HC. At first, precipitation occurs almost randomly. As time goes on, cloud activity becomes organized into propagating wavy pattern. In the end, almost all rainfall is concentrated in two wave number one structures that run in the opposite direction; because their amplitude is almost the same, we can regard it as a standing oscillation. On the other hand, rainfall distribution for the case LC, shown in Fig.2, lacks significant large scale modulation from the beginning to the end of the experiment.

The vertical distributions of latent heating realized in the two experiment (not shown here) reflected that of the specified body coolings; i.e., it was enhanced in higher levels for case HC, whereas it was enhanced in the lower levels for case LC. This is consistent with the prediction of the linear wave-CISK theories that points upper-enhanced cumulus heating as necessary factor for amplifying propagating disturbance. The spatial structure (not shown) and the phase velocity can be interpreted in the framework of linear wave-CISK theories.

b. dependence of preffered scale on surface wind speed

The case HC above gives only the lower limit of preferred scale of wave-CISK disturbances. So in order to identify the preffered scale, case HC was repeated using the 16,384 km domain model whose result is shown in Fig.3, which shows that the preffered wavelength does exsist and is about 4000km. It should be noted that this is much shorter than the preffered scale of WISHE (longer than 16000 km as shown in Nakajima,1993,1994).

The preffered wavelength was found to be sensitive to V_{sfc}, the specified wind speed in the bulk formulae used for the surface flux calculations. Fig.4 shows the result of the case where V_{sfc} = 1m/s, and Fig.5 shows that of the case with V_{sfc} = 30m/s. (I note here that V_{sfc}=3m/s in the standard cases.) Comparing Fig.3-5, we see that wavelength is longer in the case with smaller V_{sfc}, whose reason remains unclear. One possibility is that the wavelength is proportional to the period of wave that must match the PBL recovery time, which will probably be long if Vscf is smaller.

c. Failure of linear wave-CISK theories

Closely examining Fig.5 again, we notice an wave number one stationaly amplifying modulation. This type of stationaly structure becomes more evident when we further increase V_{sfc} (not shown). If one want to explain the coexsitence of propagating and statinaly modes in the linear wave-CISK theory, one must assume different proportional coefficient on cumulus heating and large scale vertical motion in propagating and stationaly modes. This exemplifies one of the limitations of linear theory, which may be useful as a framework of interpretion but can not be very useful for prediction.

Another example of the limitations of wave-CISK theory is its 'failure' in predicting the preffered scale. 'Positive-only' wave-CISK gives better prediction (growth rate flattens in the limit of long wave), but it is not sufficient. However, we must note that the prediction on the growth rate itself is not bad. In fact, even in case HC where wave number one dominates, patterns of much shorter wavelength are evident in the earlier time; i.e., shorter wave do grow faster but do not grow into very large amplitude. The same success and failure applies in the WISHE case; linear theory successfully predicts faster growth of shorter waves, but one will get false infirmation if he or she expects those waves to be dominant in the longer timescale. This type of pitfall is, in retrospect, common to usual flow instability theories.

5.Concldíng remarks

We could simulate wave-CISK type disturbances in WISHE-free surface flux condition. The phase velocity, spatial structure, and the dependence on the cloud heating parameter are consistent with the prediction of linear wave-CISK theories. Realized scale selection in terms of the finally attained wavelength is, however, significantly different from that given by the growth rate-wavelength relationship in the linear theories.

Combined with WISHE results, the wave-CISK experiments offers useful example of explicitly simulated cumulus-LS interaction. Because the real

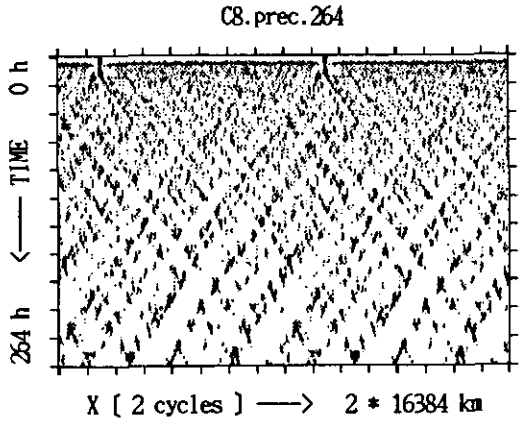

Figure 3: Time evolution of rainfall distribution in case HC in large model. Two cycles of 16,384 km domain is shown from left to roght. Time goes down from 0 h to 264 h.

observation suffers from severe undersampling, this type of study will be very important for improvement of our quantitative and qualitative understandings on the role of cumulous convection in the atmosphere. Of course the limitation that comes from the model's 2-dimensional geometry should be checked, but it must be left for studies in future, which may not be near considering the required tremendous computational resources.

Acknowledgements

Computations are done by SX-3 at NIES. The author very much thanks to the staff members of NIES, especially Dr.Numaguti, for the technical help in usage of the SX-3 system.

References

1. Nakajima, K. (1994): Direct simulation of large scale organizations of cumulus convection. Ph.D Dissertation at University of Tokyo. 144p. (in Japanese. English version will be available from author.)

2. Nakajima, K. (1993): Ultra-high resolution modeling of the tropical atmosphere. CGER'S SUPERCOMPUTER ACTIVITY REPORT 1992., pp.8-9.

3. Yamasaki,M. (1969): Large-scale disturbances in the conditionally unstable atmosphere in low latitudes. Pap.Meteor.Geophys., 20, 289-336.

4. Hayashi,Y. (1970): A theory of large-scale equatorial waves generated by condensation heat and accelerating the zonal wind. J.Meteor.Soc.Japan, 48,140-160.

5. Lindzen,R. (1974): Wave-CISK in the tropics. J.Atmos.Sci.,31,156-179.

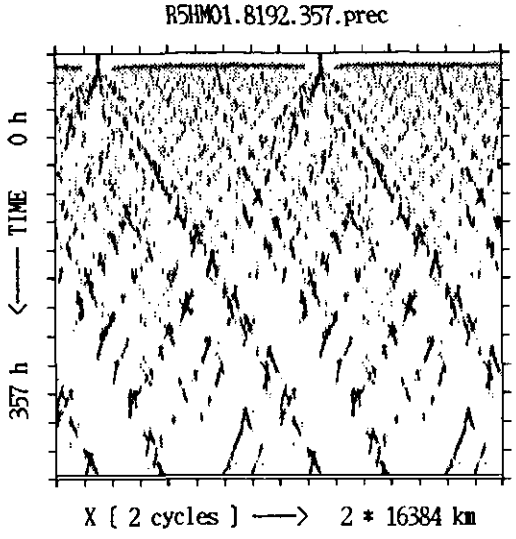

Figure 4: Same as Fig.3 but for the case with V_{sfc} = 1 m/s. Time goes down from 0 h to 357 h.

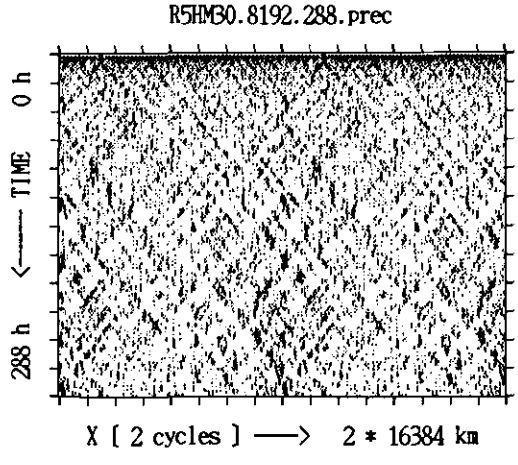

Figure 5: Same as Fig.3 but for the case with V_{sfc} = 30 m/s. Time goes down from 0 h to 288 h.

Development of an Atmospheric General Circulation Model for Climate Research

Contact Person	Atusi Numaguti Atmospheric Environment Division, National Institute for Environmental Studies, Japan Environmental Agency.
Research Organization	Seiji Sugata, Shigeki Mitsumoto National Institute for Environmental Studies Masaaki Takahashi, Toshiro Kumakura, Teruyuki Nakajima, Akimasa Sumi, Taroh Matsuno Center for Climate System Research, University of Tokyo.

Keywords climate model, atmosphere, parameterization, radiation, land surface, clouds

1 Background

A quantitative evaluation of climate change such as the global warming is impossible without a high-quality numerical model which describes the dynamics of the climate system and the circulations of the energy and material. The purpose of this research is to develop a community climate model which enables research into mechanism of the climate change with the time scales ranging from several years to hundreds of years.

At the present time, there are about five comprehensive atmosphere-ocean combined climate models in the world. Also, the atmospheric general circulation models are developed at about ten organizations and are used for the experiment of carbon dioxide doubling. These models give qualitatively similar results for the global warming prediction, but do not coincide quantitatively with one another. For example, the global average of the temperature rise at CO_2 doubling varies from 2°C to 5°C depending on the models. In addition, the ability of each model in reproducing the current climate is not satisfactory. For example, the ocean-atmosphere coupled models cannot yield realistic climate maps without making an artificial adjustment of the flux between atmosphere and ocean. These problems are attributed to the incomplete representation of physical processes and limited spatial resolution.

Under these circumstances, this project of the development of a climate model and improvement of the representation of physical processes is started toward the quantitative estimation of the climate change.

2 Objective

The goal of our research is the quantitative estimation of the climatic change using a comprehensive climate model of atmosphere-ocean-land climate system. Currently, we are developing a atmospheric part of the model, *i.e.*, an atmospheric general circulation model (AGCM).

The basic standpoint in the development is to make the model based on obvious physics and possibly less dependent on empirical parameters. Effective model code was employed to make the long-term run possible with high resolution. In addition, considerable attention was paid to the readability and module compatibility of the code to enable a community use of the model.

The model is based on a simple AGCM developed at University of Tokyo [1]. In order to make the model suitable for climate research, developments on the following three points are required. The first is the improvement of the parameterization of physical processes. Particularly, the parameterizations of radiative transfer, cloud precess, and land-surface processes are very important. The second is the preparation of dataset for use of the model as boundary condition. The third is the testing on the model ability for reproducing the current climate and the tuning of the model parameters, the parameterization schemes, and the boundary conditions.

3 Model Description

The outline of the current model is summarized as the followings.

Basic Equations: 3-dimensional hydrostatic primitive equations on sphere with normalized pressure (σ) coordinate.

Prognostic Variables: Horizontal velocity, temperature, surface pressure, total water content, soil temperature, soil moisture, snow depth.

Discretezation: Spectral transformation method with Gaussian grid in horizontal and an grid differentiation [2] in vertical. Leap-frog scheme is used for time integration.

Resolution: Variable, currently tested with T42 (2.8° grid) 20 levels and T21 (5.6° grid) 20 levels.

Physical Processes: k-distribution model for radiative transfer [3].
Arakawa-Schubert [4] type cumulus parameterization with prognostic closure.
Estimation of cloud liquid water by prognostics

of the total water content [5].
Mellor-Yamada [6] level 2 turbulence scheme.
Simple non-local diffusion scheme.
Bulk scheme for surface fluxes [7].
Multi-layer treatment of land-surface energy budget and hydrology [8].
Gravity-wave drag scheme [9].

4 Results

4.1 Seasonal Climatology Experiment

Introducing physical parameterizations reported above, the model was run under realistic boundary conditions for long times (about 10 year) and the results were compared with observed climatology fields. The adopted horizontal resolutions is T21(equivalent grid size 5.5°) or T42(3°) and vertical resolution is 20 levels.

The zonally averaged distribution of temperature of T21 run and its deviation from observed climatology is shown in Fig.1 for three month average from June to August. The deviation is less than two degrees in most part of the troposphere. However, there is large cold bias near the tropopause region, especially near the pole.

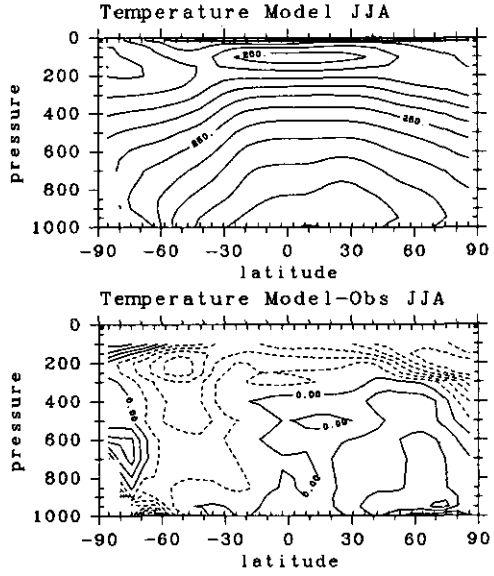

Fig.1 Distribution of zonal mean temperature (upper) and its deviation from observed climatology (lower). Three month average from June to August is shown. Contour interval is 10K(upper) and 2K(lower).

The distribution of precipitation is shown in Fig.2. The location and strength of the large-scale precipitation area is well simulated.

By examining the model result, it is found that the model reproduces fairly realistic climate except for some problems, for example, too dry tropical middle troposphere and too moist upper troposphere (Fig.3) and small precipitation in Amazon region in austral summer.

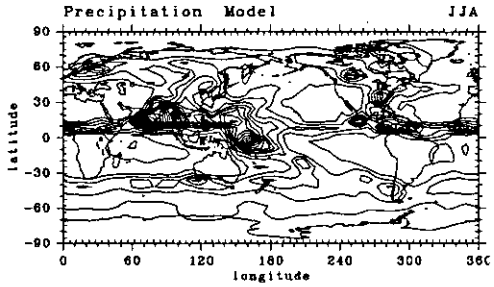

Fig.2 Distribution of precipitation. Three month average from June to August is shown. Contour interval is 50mm/month.

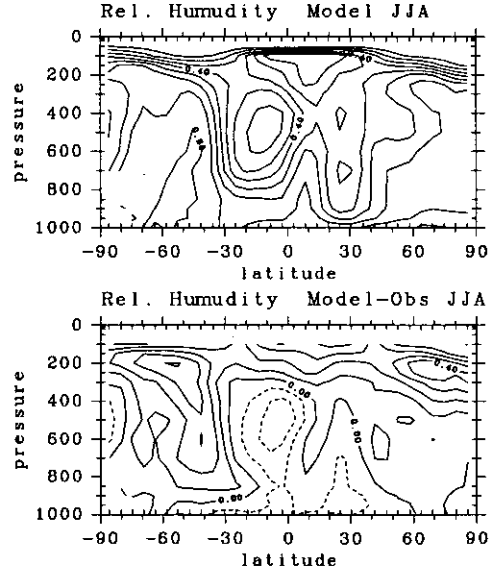

Fig.3 Distribution of zonal mean relative humidity (upper) and its deviation from observed climatology (lower). Three month average from June to August is shown. Contour interval is 10%.

4.2 Development of parameterization schemes

Development of efficient radiation code: In order to solve the transfer equation efficiently, the Discrete Ordinate/Adding method is adopted in our scheme. However, the number of channels of absorption that the model computes is extremely limited even with the scheme. We have overcome this difficulty by adopting k-distribution method and by applying a nonlinear optimization scheme for the selecting the channels. As the result, we can reduce the number up to 48 from 242 keeping the error of the heating rate to be smaller than 0.5 ° K/day below 40 km altitude [3].

Cloud liquid water content prediction: In order to express the feedback process concerning the cloud

optical thickness appropriately, an scheme for the prediction of cloud liquid water content is developed. In this scheme, the predicting variable is the total water content. The liquid water is diagnosed assuming the variability of the total water within the grid. The precipitation and evaporation of rain is estimated by simplified Kessler type formula. It is confirmed the scheme successfully reproduce the observed long and short radiative fluxes at the top of the atmosphere.

Modified Arakawa-Schubert cumulus parameterization: An Arakawa-Schubert type cumulus parameterization is developed. The mass flux is prognostically estimated using cloud work function. The effect of downdraft is incorporated in a rather simple manner.

Improved treatment of boundary layer processes: The effect of cloud is incorporated in the vertical diffusion process by use of moist Richardson number. In the surface flux parameterization, the effect of free convective motion is incorporated to improve the evaporation field over the tropical ocean. The effect of non-local diffusion in the boundary layer is also incorporated.

Sensitivity study with soil model: Aiming to the development of comprehensive land surface model in use of climate model, a simple sensitivity study are done using an one-dimensional model of land surface [8]. A one-dimensional soil model with explicit treatment of ground water table was developed. The model is based on thermal diffusion equation and Richards' equation for soil water. The model was coupled with a simple model of atmospheric boundary layer and was run for long time with various conditions of precipitation and radiation as external forcing. The result indicates the importance of appropriate treatment of the deep water and runoff in the long-term behavior of the land surface.

Incorporation of vegetation effect: An attempt in incorporating the effect of vegetation into the land surface model is done basically following the SiB model [10]. Results of one dimensional simulation with and without the effect of transpiration and interception show significant difference in the seasonal pattern of evaporation.

5 Summary

An atmospheric general circulation model for use of the climate study is developed and tested in the ability reproducing the present climate. The result is generally good, except for some problems probably due to inadequateness of physical parameterization. The improvement of the parameterization schemes, particularly for the cloud-radiation interaction and land surface processes is required. Also, more comprehensive test of the model performance not only for the averaged climate but also for the variability is needed for the validation and further improvement of the model.

6 Acknowledgments

This research is supported by Global Environment Research Program of Japan Environmental Agency. Assistance by Dr. A. Abe-Ouchi, Messrs. M. Tsukamoto, S. Emori, and T. Nishimura is greatly appreciated.

References

1. A. Numaguti, *J. Atmos. Sci.*, **50**, 1874–1877 (1993)
2. A. Arakawa A. and M.J. Suarez, *Mon. Weather Rev.*, **111**, 34–45 (1983)
3. T. Nakajima and M. Tsukamoto, *in preparation* (1994)
4. A. Arakawa and W.H. Schubert, *J. Atmos. Sci.*,, **31**, 671–701 (1974)
5. H. Le Treut and Z.-X. Li, *Climate Dynamics*, **5**, 175–187 (1991)
6. G.L. Mellor and T. Yamada, *J. Atmos. Sci.*, **31**, 1791–1806 (1974)
7. J. Louis, *Bound. Layer Meteor.*, **17**, 187–202 (1979)
8. S. Mitsumoto, S. Emori and K. Abe, *J. Japan Soc. Hydrol. Water Res.* , **7**, 259–267 (1994)
9. N.A. McFarlane, *J. Atmos. Sci.*, **44**, 1775-1800 (1987)
10. P.J. Sellers, Y. Mintz, Y.C. Sud, A. Dalcher, *J. Atmos. Sci.*, **43**, 305–331 (1986)

A role of Hadley circulations and baroclinic waves in the global angular momentum budget

Contact Person Masaki Satoh
Department of Mechanical Engineering, Saitama Institute of Technology
Okabe, Saitama, 369-02, Japan

Keywords Hadley circulation, baroclinic waves, axisymmetric model, angular momentum budget

1. Introduction

Observationally, it is well known that the Hadley cells in the low-latitudes and the Ferrel cells as a zonal average of baroclinic waves in mid-latitudes play important roles in the angular momentum budgets of the general circulation [1]. Theoretical understandings of the Hadley circulations are promoted by using axisymmetric models [2,3]. It is not sufficiently known, however, to what extent these symmetric circulations describe more realistic asymmetric ones. Williams [4,5] has compared axisymmetric circulations with asymmetric ones by using a general circulation model (GCM). However, it is difficult to extract general conclusions from his results, since he used the "swamp" condition as the surface boundary condition [6]. It is the aim of this study to calculate symmetric and asymmetric circulations with GCM under the prescribed surface temperature distribution, so as to investigate roles of the Hadley and Ferrel cells in the angular momentum budgets, particularly through dependencies on the rotation rates.

2. Model

The GCM developed at the University of Tokyo [7] is used to calculate asymmetric and axisymmetric states (here after, 3D and 2D, respectively). The resolution of 3D is T42 and 16 layers. In 2D, the modes of wave number zero alone are used in longitudinal direction. The moist adjustment scheme, a simple non-gray radiation model, and the level II of Yamada and Meller boundary layer schemes are used as physical processes. The surface temperature is prescribed as $300\mathrm{K} - 40\mathrm{K} \times \sin^2\varphi$ (φ is latitude), and the surface is assumed to be wet (an aqua planet model). Integrations are started from a state at rest with a uniform temperature 250K. An equilibrium state of 3D is defined by a mean of 80 – 160 days, whereas one of 2D by a mean of 200 – 400 days. Dependencies on rotation rates Ω are examined: $\Omega/\Omega_0 = 3$, 1 and 1/3, where Ω_0 is the rotation rate of the earth.

3. Results

Figs. 1 (a)–(c) show meridional distributions of zonal winds for 2D. At the equator, zonal winds are easterly from the surface to the upper troposphere, while in the mid- and high-latitudes they are westerly except for the bottom layers. The width of the equatorial easterly are smaller as Ω is larger. Easterlies develop in the low-latitudes where direct cells (the Hadley cells) exist. In the mid- and high-latitudes, a multiple cellar structure (symmetric cells) exists. The moving symmetric cells will no longer exist in 3D; the Richardson number of the averaged state of the mid-latitudes is approximately 10, so that it is in a baroclinic unstable regime [8].

Figs. 1 (d)–(f) show meridional distributions of longitudinal mean zonal winds for 3D. At the equator, there are easterlies in the lower layers, while westerlies in the upper troposphere. These westerlies are not so strong that they form a jet (a maximum of westerly). In the mid-latitudes, westerlies prevail from the top to the bottom layers. Because of the existence of baroclinic waves, angular momentums are effectively transported downward in comparison to 2D. The surface winds near the poles are easterlies for $\Omega/\Omega_0 \geq 1$, where polar direct cells exist.

4. Discussion and further comments

The mass fluxes of the Hadley circulation of 3D, Ψ_H, can be approximately expressed in terms of the external parameters by using the simple Hadley models of 2D [3,6], although they are more or less larger than those of 2D,

The mass fluxes of the Ferrel cells in 3D, Ψ_F,

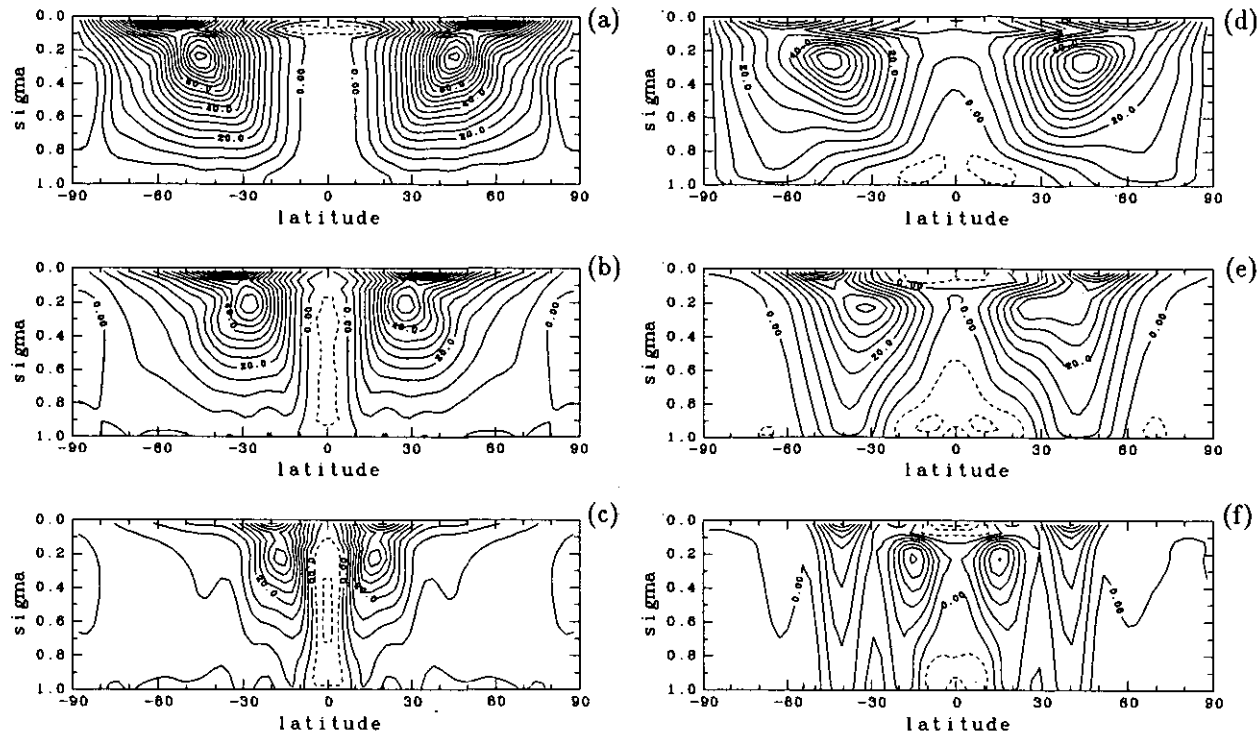

Fig. 1. Meridional distributions of zonal winds for (a) 2D, $\Omega/\Omega_0 = 1/3$, (b) 2D, $\Omega/\Omega_0 = 1$, (c) 2D, $\Omega/\Omega_0 = 3$, (d) 3D, $\Omega/\Omega_0 = 1/3$, (e) 3D, $\Omega/\Omega_0 = 1$, and (f) 3D, $\Omega/\Omega_0 = 3$. Contour intervals are 5 m/s.

are related with those of the Hadley cells through the angular momentum budgets. The upward transports of the angular momentum in the Hadley cells are balanced by the downward ones in the Ferrel cells, so that one may have

$$\frac{\Psi_F}{\Psi_H} = -\frac{\Delta l_H}{\Delta l_F} = -\frac{\Delta\varphi_H}{2\Delta\varphi_F} \approx -\frac{1}{2}, \qquad (1)$$

where Δl_H, Δl_F are differences of the angular momentums between the upward and downward branches in the the respective cells. Their absolute components are related with the latitudinal widths of the cells, $\Delta\varphi_H$, $\Delta\varphi_F$, where $\Delta\varphi_H \approx \Delta\varphi_F$ can be assumed as in Eq. (1).

One may also discuss the relations between the Hadley cells and the amplitudes of the baroclinic waves and the latitudinal energy transports by the baroclinic waves by using theories of baroclinic instability. This picture will give another point of view for the life cycle of cyclones and the estimation of heat transport in energy budget models.

Acknowledgments

Figures were produced by GFD-DENNOU libraries and GTOOL3 by Dr. Numaguti.

References

1. E. Palmen and W. Newton, *Atmospheric Circulation Systems*, Academic Press, 603pp (1969)
2. E. K. Schneider, *J. Atmos. Sci.*, **34**, 280-296 (1977)
3. I. M. Held and A. Y. Hou, *J. Atmos. Sci.*, **37**, 515-533 (1980)
4. G. P. Williams, *Climate Dynamics*, **2**, 205-260 (1988)
5. G. P. Williams, *Climate Dynamics*, **3**, 45-84 (1988)
6. M. Satoh, *J.Atmos. Sci.*, **51**, 1947-1968 (1994)
7. A. Numaguti, *J. Atmos. Sci.*, **50**, 1874-1887 (1993)
8. P. H. Stone, *J. Atoms. Sci.*, **23**, 390-400 (1966)

The study of mass transport between the troposphere and stratosphere

Contact Person Isamu Yagai
Meteorological College, Meteorological Agency of Japan.

(Research Organization) Koji Yamazaki
Masaru Chiba
Kiyotaka Shibata
Tatsusi Tokioka
Akira Noda
Meteorological Research Institute

Key Words ozone, mass transport, the troposphere and stratosphere ,sea surface temperature, global warming

1. Backgrounds

Predicting climate change due to an increase in atmospheric carbon dioxide was first studied using simplified one-dimensional models such as radiative-convective models. These models, however, could not represent the horizontal transport of heat, water vapor, ozone and other substances. Therefore, the three-dimensional general circulation developed at the Meteorological research Institute (MRI) is used in this study to asses the influence of the global warming to the transport of ozone.

2. Objective

In order to simulate the current distribution of ozone well, we will make improvement of the MRI GCM. Furthermore, we will estimate the effect of global warming to the redistribution of ozone.

3. Method

The first is the perpetual July experiment by the 12 layer MRI GCM with the $\pm 2°C$ SST (Sea surface temperature) perturbations. This was time integrated for 90 days and the last 30 days were analyzed. The results with the global sensitivity and surface fluxes are presented by Cess et al. (1991)[1] and Randall et al. (1992)[2].

The second is the seasonal run by the 12 layer GCM which is started from the atmospheric condition at 12Z 15 December 1982. Stratospheric sudden warmings appear in the course of the experiment. The simulated zonal mean ozone mixing ratio are compared with the observation.

We have developed 15 layer version of the MRI GCM by increasing the vertical resolution in the troposphere. The 15 model levels are approximately 1.39, 2.68, 5.18, 10.0, 19.3, 37.3, 72.0,119, 168, 237, 335, 457, 589, 741, 912 hPa, while the 12 layer model has 5 levels in the troposphere corresponding approximately to 150, 300, 500, 700, and 900 hPa. The model was started from 00Z 1 January 1979 and time integrated for 3 years. The distribution of sea surface temperature is prescribed based on climatological data (Climate RUN). In addition we completed another experiment where the zonally uniform SST anomaly was added to the climatological value and the concentration of the carbon dioxide was doubled (Warming RUN).

4. Results

In the perpetual July experiment, the ozone in the stratosphere decreased while the ozone in the troposphere increased in the $+2°C$ SST perturbation experiment. This result is caused by dynamical effects since the zonally integrated photochemical ozone production rates tend to increase ozone in the stratosphere.

In the seasonal run by the 12 layer GCM, stratospheric sudden warmings appear in the course of the experiment. The simulated zonal mean ozone mixing ratio is compared with the observation. The maximum value and the height over the equator is almost coincide with the observation. Simulated ozone in the this experiment increases in the middle stratosphere while it decreases in the upper stratosphere due to the advective process during the sudden warmings.

Figure 1 shows the zonal mean ozone mixing ratio (ppm) in parts per million by mass for January by the 15 layer GCM. The maximum value and its height over the equator is almost coincide with the observation.

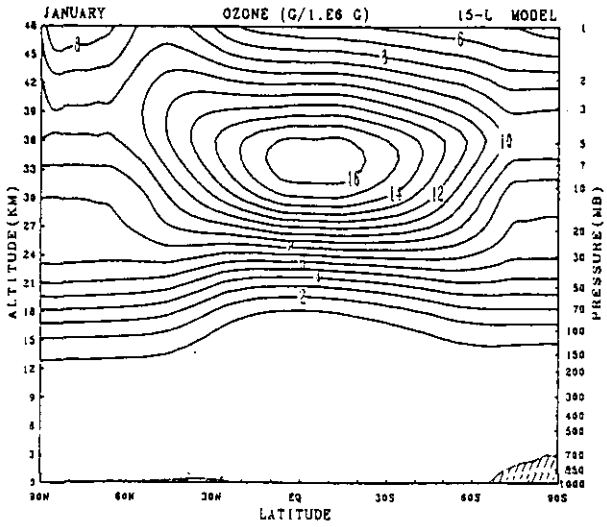

Figure 1: Zonally and monthly averaged ozone mixing ratio (ppm) by the 15 layer MRI GCM (Climate RUN).

Figure 2 shows the difference of ozone mixing ratio for January between Climate RUN and Warming RUN. Figure 3 is the same as figure 2 but for the ozone photochemical production rate. The ozone decreases in the upper stratosphere at polar night region, while the ozone increases around 60 °N in the upper stratosphere. The change of ozone in this region is caused by the dynamical process, while at lower latitudes in the stratosphere ozone increases by the photochemical process through the change of temperature in this region. These results, however, have to be checked in the analysis of longer period since the model as well as real atmosphere has considerable variation on interannual time scales.

Reference

Cess, R.D., G.L. Potter, M.-H . Zhang, J.P. Blanchet, S. Chalita, R. Coloman, D.A. Dazlich, , A.D. Del Genio, V. Dymnikov, V. Galin, D. Jerrett, E. Keup, A.A. Lacis, H.Le. Treut, Z.-X. Li, X.-Z. Liang, J. F. Mahfouf, B.J. McAvaney, V.P. Meleshko, J.F.B. Mitchell, J.-J. Morcrette, P. M. Norris, D.A. Randall, L. Rikus, E. Roeckner, J. F. Royer, U. Schlese, D.A. Sheinin, J.M. Slingo, A.P. Sokolov, K.E. Taylor, W.M. Washington, R.T. Wetherald, and I. Yagai, : Interpretation of snow-climate feedback as produced by 17 General Circulation Models. Science, 253, 888-892, 1991.

D.A. Randall, R.D. Cess, J.P. Blanchet, G.J. Boer, D.A. Dazlich, A.D. Del Genio, M. Déqué, V. Dymnikov, V. Galin, S.J. Ghan, A.A. Lacis, H.Le. Treut, Z.-X. Li, X.-Z. Liang, B.J. McAvaney, V.P. Meleshko, J.F.B. Mitchell, J.-J. Morcrette, G.L. Potter, L. Rikus, E. Roeckner, J.F. Royer, U. Schlese, D.A. Sheinin, J. Slingo, A.P. Sokolov, K.E. Taylor, W.M. Washington, R.T. Wetherald, I. Yagai, and M.-H . Zhang, : Intercomparison and Interpretation of surface energy fluxes in atmospheric general circulation models. J. Geophys. Res., 97, 3711-3724, 1992.

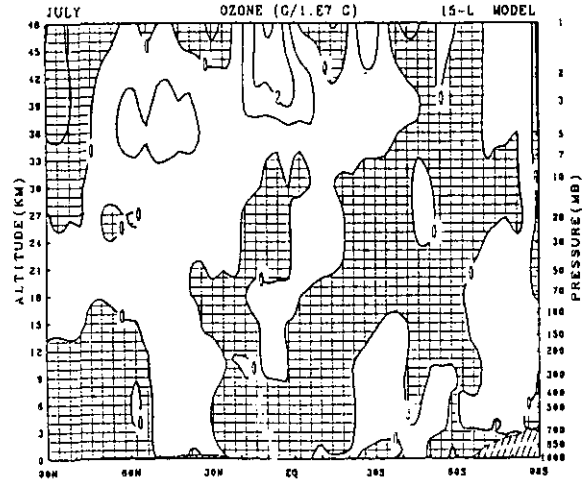

Figure 2: The difference of ozone mixing ratio (0.1 ppm) for January, Warming RUN-Climate RUN. Negative values are shaded.

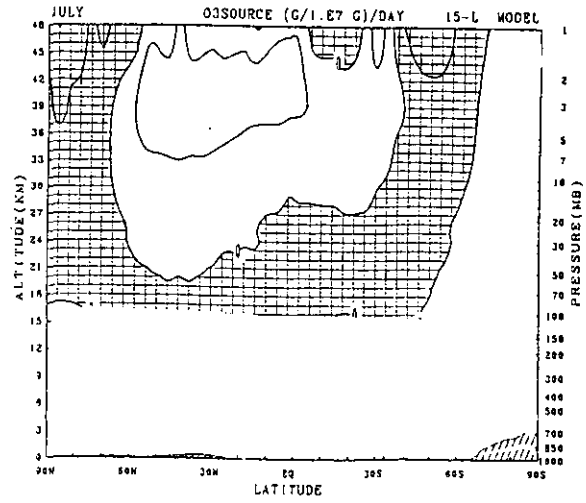

Figure 3: The difference of ozone photochemical production rate (0.01 ppm/day) for January, Warming RUN-Climate RUN. Negative values are shaded.